

## Article

# The Influences of O<sub>2</sub> Availability on the Microbial Activities and Fe Transformations in the Iron Formation Caves of the Southern Espinhaço Range, Brazil

Melissa K. Mulford<sup>1,2</sup>, Anela Mukherjee<sup>2</sup>, Augusto S. Auler<sup>3</sup> , Hazel A. Barton<sup>4,\*</sup> and John M. Senko<sup>1,2,5</sup>

<sup>1</sup> Integrated Bioscience, University of Akron, Akron, OH 44325, USA; mkm118@uakron.edu (M.K.M.); senko@uakron.edu (J.M.S.)

<sup>2</sup> Department of Biology, University of Akron, Akron, OH 44325, USA; anelam19@gmail.com

<sup>3</sup> Instituto do Carste/Carste Ciência Ambiental, Belo Horizonte 30360-260, MG, Brazil; aauler@gmail.com

<sup>4</sup> Department of Geological Sciences, University of Alabama, Tuscaloosa, AL 35847, USA

<sup>5</sup> Department of Geosciences, University of Akron, Akron, OH 44325, USA

\* Correspondence: hbarton1@ua.edu; Tel.: +1-205-348-0818

**Abstract:** Over 3000 iron formation caves (IFCs) have formed in erosion-resistant Fe(III)-rich rocks throughout Brazil. Microbial Fe(III) reduction occurs in IFCs, where a microbe-rich, Fe(III)-depleted paste (*sub muros*) is found behind an Fe(III)-(hydr)oxide crust in the ceiling/walls. Microbial Fe(III) reduction in *sub muros* appears to be responsible for the transformation of Fe(III) to more soluble Fe(II), which is removed, leading to cave formation. This process of biospeleogenesis is likely controlled by O<sub>2</sub> availability, which is linked to seasonal changes. Here, we studied the effects of alternating anoxia/oxia on the microbial community and on Fe solubility in banded iron formation (BIF), a rock type consisting of layered Fe(III)-oxide and silicate. Incubations of synthetic pore water, pulverized BIF, and *sub muros* were prepared and incubated under anoxia, during which BIF-Fe(III) reduction proceeded. During the Fe(III) reduction period, Firmicutes and/or Alphaproteobacteria were enriched, and genes involved in Fe(III) and sulfate reduction were detected in the metagenomes. Fe(II) oxidation genes, which were detected in the fresh *sub muros*, were not found. Upon the addition of atmospheric O<sub>2</sub>, Fe(III) reduction was arrested, and incomplete Fe(II) oxidation occurred. Betaproteobacteria, Gammaproteobacteria, and Chloroflexi increased in relative abundance following aeration, and Fe(III) reduction genes were still identified. Our results demonstrate that the *sub muros* microbial community retains the ability to reduce Fe(III) and drive speleogenesis despite fluctuations in O<sub>2</sub> levels.

**Keywords:** cave; iron reduction; iron oxidation; banded iron formation; geomicrobiology



**Citation:** Mulford, M.K.; Mukherjee, A.; Auler, A.S.; Barton, H.A.; Senko, J.M. The Influences of O<sub>2</sub> Availability on the Microbial Activities and Fe Transformations in the Iron Formation Caves of the Southern Espinhaço Range, Brazil. *Minerals* **2024**, *14*, 425. <https://doi.org/10.3390/min14040425>

Academic Editor: Yul Roh

Received: 12 March 2024

Revised: 10 April 2024

Accepted: 17 April 2024

Published: 20 April 2024



**Copyright:** © 2024 by the authors. Licensee MDPI, Basel, Switzerland. This article is an open access article distributed under the terms and conditions of the Creative Commons Attribution (CC BY) license (<https://creativecommons.org/licenses/by/4.0/>).

## 1. Introduction

The Carajás Ridge, Southern Espinhaço Range, and Iron Quadrangle regions of Brazil consist of extensive deposits of Fe(III)-rich rocks, including banded iron formation (BIF) and the overlying duricrust, canga. BIF comprises 54–70 wt% Fe(III) oxide minerals, such as hematite (Fe<sub>2</sub>O<sub>3</sub>), and 25–45 wt% silicate minerals [1–4], while canga is primarily composed of fragments of BIF cemented by goethite (FeO(OH)) and is 89 wt% Fe(III) oxide [3,5]. These three regions are home to over 3000 iron formation caves (IFCs) that have formed in BIF and canga, even though these rocks are highly resistant to erosion [6]. Both BIF and canga are composed of minerals that are poorly soluble and resistant to dissolution weathering [7]. Because Fe(III)-(hydr)oxides are relatively insoluble in water with a pH above 3.5, and the water in and around these IFCs is typically circumneutral in pH, Fe(III) must be reduced to relatively soluble Fe(II) to be mobilized and allow for the formation of the observed IFCs.

Recent evidence has demonstrated that Fe(III)-reducing microorganisms (FeRMs) may be responsible for the reduction in poorly soluble Fe(III)-oxides in the host rock to Fe(II),

supported by organic carbon from the terrestrial surface [4,8–14]. This was supported by the identification of active FeRM within the caves [4,14] and the presence of a Fe(III)-depleted material (termed *sub muros*) behind the IFC walls [14]. *Sub muros* was found behind an Fe(III)-(hydr)oxide crust, which forms as a result of oxidation of the outermost exposed Fe(II) in the *sub muros* and the precipitation of Fe(III)-(hydr)oxide phases to form the crust [14]. This Fe(III)-(hydr)oxide crust is thought to create an O<sub>2</sub> barrier, limiting O<sub>2</sub> intrusion into the *sub muros* and allowing Fe(III) reduction to proceed, with the resulting Fe(II) being removed via groundwater. The removal of Fe(II) may be enhanced by chemical interactions that stabilize Fe(II) by forming a mobile Fe-Si colloid [15], although the effects of these chemical interactions have not been studied in IFC environments. Fe(III) reduction continues until the oxide crust is unable to support the *sub muros* and collapses into the cave, causing enlargement. The collapse of the crust leads to the oxidation of Fe(II) in the freshly exposed *sub muros*, creating a new Fe(III)-oxide crust in place and facilitating another cycle of reductive solubilization of Fe(III). This novel cave genesis process has been termed exothermic biospeleogenesis [14].

The climates of the IFC regions of Brazil are tropical subhumid with wet and dry seasons [3,11,16]. Fe(III) reduction is thought to be stimulated during the wet season when organic matter is more readily available, as suggested by a recent study of Lake Violão in Carajás, Brazil [17]. During the dry season, canga exposed at the surface experiences Fe(II) oxidation, which stabilizes the canga and limits erosion [3,11,17]. Our prior work has also demonstrated that the Fe(II) is mobilized by cycles of hydrologic flow, which appears to remove Fe(II) and increase the rate of Fe(III) reduction [13]. The removal of Fe(II) may be enhanced by interactions with silica, which prevents Fe(II) oxidation through sorption/complexation interactions [15,18,19].

If our hypothesis of episodic speleogenesis is correct, the microbial community is exposed to cycling anoxic and oxic conditions, both on a seasonal scale (wet/dry seasons) and on a more localized, irregularly timed scale (wall collapse). Additionally, the exposure of biogenic Fe(II) to oxic waters could limit Fe export. The aim of this study was to determine the structural and metabolic dynamics of *sub muros*-associated microbial communities under alternating anoxic and oxic conditions. To achieve this, we examined the *sub muros* when incubated with the host rock (BIF) under alternating anoxic and oxic conditions to mimic the fluctuations in water and the O<sub>2</sub> availability associated with the cave-hosting systems [8,14,17]. Our results show that the *sub muros* microbial community is affected by anoxic to oxic shifts while continuing to maintain the ability to reduce Fe(III) in BIF, but it does not oxidize the generated Fe(II) extensively. These data suggest that microbial Fe(II) oxidation within these environments may be inhibited by interactions with silica, enhancing Fe(II) mobilization in IFCs, even during periods of high O<sub>2</sub> availability.

## 2. Materials and Methods

### 2.1. Sample Collection and Preparation for Incubations

*Sub muros* material and BIF samples were obtained from IFCs in the Southern Espinhaço Range, Minas Gerais, Brazil in December 2018 during the wet season. Two BIF samples were collected from the ceilings and walls of two caves' interiors prior to destruction through mining and placed in sterile aluminum foil for transport. These caves were located at altitudes of 684 m and 662 m. BIF was prepared by first breaking up the large, friable samples with a rock hammer. BIF fragments were then powdered using a ball mill (SPEX Industries, Inc., Metuchen, NJ, USA) until all of the material passed through a 4 mm sieve. The powdered BIF was then sterilized by autoclaving at 121 °C for 30 min, cooling for 30 min, and then autoclaving again to ensure the deactivation of endospore-forming bacteria. This method of microbiological deactivation appeared to be sufficient for sterilizing canga in a previous experiment, as DNA could not be extracted, and no cells were detected in uninoculated incubations [4,13]. The sterilized BIF was then dried at 65 °C for 14–16 h in an oven. The mineral composition of BIF was analyzed using X-ray diffraction and energy-dispersive X-ray analysis, which revealed that the BIF is 65% quartz and 35%

hematite by weight (Supplementary Information). The *sub muros* material was collected from another IFC, located at 846 m altitude (also in December 2018), by first removing the Fe(III)-oxide crust layer and then using a sterile garden shovel to place the material in sterile glass jars, which were then sealed with plastic tape to minimize contact with O<sub>2</sub>. *Sub muros* samples were stored at 4 °C upon returning from the field.

### 2.2. Batch Experiments and Fe(II) Measurement

Incubations were prepared in a Coy anaerobic glove bag (Coy Laboratory Products, Inc., Grass Lake, MI, USA) filled with 1–3% H<sub>2</sub>, balance N<sub>2</sub>. The synthetic pore water (SPW) formulation was based on the characterization of IFC porewaters and consisted of 5 mM CaCl<sub>2</sub>, 0.1 mM Na<sub>2</sub>SO<sub>4</sub>, and 0.1 mM KH<sub>2</sub>PO<sub>4</sub>, adjusted to a pH of 6.8 [13]. Sodium lactate (5.0 mM) was included as an electron donor and carbon source. SPW was sterilized by autoclaving at 121 °C for 25 min. O<sub>2</sub> was removed from the SPW by bringing the solution to near boiling while under a stream of filter-sterilized N<sub>2</sub> gas (0.2 µM Corning Incorporated, Oneonta, NY, USA) for 45 min, and then it was allowed to cool under a stream of N<sub>2</sub> gas. The SPW was then transferred to the anaerobic glove bag. Batch incubations were prepared in 160 mL serum bottles with 20 g BIF [equivalent to approximately 36 mmol Fe(III)] and 60 mL anoxic SPW. Where appropriate, 5 g *sub muros* material was added as an inoculum. Abiotic controls did not receive *sub muros*. Serum bottles were sealed with butyl rubber stoppers held in place with aluminum crimp seals. Incubations were carried out in replicates of three (sterile controls), four (oxic incubations), or six (anoxic incubations) to account for the heterogeneity of *sub muros* and BIF.

Samples were collected from incubations using a needle and syringe in the Coy anaerobic glove bag. Samples taken for total Fe(II) quantification were placed in 0.5 M HCl. After extraction for 16–24 h, samples were then centrifuged at 12,100× g for 5 min to separate solids from solution. Fe(II) in this solution was then quantified by ferrozine assay [20]. Samples taken for dissolved Fe(II) quantification were centrifuged at 12,100× g for 5 min to separate solids from solution, and then the supernatant was placed in 0.5 M HCl. Dissolved Fe(II) in this solution was then quantified by ferrozine assay. To observe the effects of anoxic/oxic cycling on the community and Fe oxidation state, selected incubations were flushed with 3–6 headspace volumes of filter-sterilized (0.2 µm) air after 91 days of anoxia, with headspace replacement weekly for the remainder of the experiment.

### 2.3. 16S rRNA Gene Sequencing and Analysis

Genomic DNA was extracted from the samples using the DNeasy PowerLyzer Power-Biofilm Kit (Qiagen, Germantown, MD, USA). Subsamples from the replicate incubations were pooled before DNA extraction. Two replicates from anoxic and oxic incubations were prepared. PCR amplification of the 16S rRNA V4 region using the 515F (5'-GTG CCA GCM GCC GCG GTA A-3') and 806R (5'-GGA CTA CHV GGG TWT CTA AT-3') primers [21] was performed using unique barcodes along with Illumina adapter sequences (Integrated DNA Technologies, Coralville, IA, USA). Amplification was performed using a Mastercycler Nexus Gradient (Eppendorf, Enfield, CT, USA) with a 3 min 94 °C hot start, followed by 30 cycles of denaturing at 94 °C for 45 s, annealing at 50 °C for 60 s, and then a 72 °C extension for 90 s, followed by a final extension step at 72 °C for 10 min. The PCR products were gel-purified and quantified using a Qubit dsDNA HS Assay Kit (Life Technologies, Waltham, MA, USA). Samples were then sequenced on an Illumina MiSeq with paired-end 250 bp reads. Taxonomic assignments were determined by processing the raw sequences through QIIME 2 2020.2 [22] using the q2 quality filter and deblur plugins for the quality filter [23,24] and the q2-feature-classifier plugin [25,26] called classify sklearn taxonomy classifier, which was trained against the Greengenes 18\_8 99% OTUs reference sequences to assign taxonomies to the raw sequences [25,27]. Figures were produced using the ggplot2 [28] and RColorBrewer [29] packages in R 4.1.1 [30].

#### 2.4. Shotgun Metagenomic Sequencing and Analysis

For metagenomic DNA sequencing, genomic DNA was extracted from the samples as described. Subsamples from batch incubation replicates were pooled before DNA extraction. Libraries were prepared using Illumina DNA Prep, (M) Tagmentation library preparation kit (Illumina, San Diego, CA, USA) [31] following the manufacturer's user guide. Initial DNA concentrations were evaluated using the Qubit dsDNA HS Assay Kit (Life Technologies, Waltham, MA, USA). Because of the low DNA yield from the oxic incubation, whole-genome amplification was performed using the REPLI-g Midi Kit (Qiagen, Germantown, MD, USA). The linear amplified DNA was then cleaned using DNEasy PowerClean Pro Cleanup Kit (Qiagen, Germantown, MD, USA), and the DNA concentration was analyzed again. Libraries were prepared for each sample by using 30–50 ng DNA, which underwent simultaneous fragmentation and addition of adapter sequences. These adapters were used during a limited-cycle PCR in which unique indices were added to the sample. Following the library preparation, the libraries were pooled in equimolar ratios of 0.6 nM and sequenced paired-end for 300 cycles using the NovaSeq 6000 system (Illumina).

The raw metagenomic reads were then trimmed, assessed, assembled into contigs, quality-assessed, binned into putative genomes, quality-assessed again, and quality-filtered ( $\geq 80\%$  completeness and  $\leq 10\%$  contamination). Bins were extracted as assemblies and taxonomies of both metagenome-assembled genomes (MAGs), and raw reads were assigned using Kbase 2.6.4 [32]. The following applications were used for each step, respectively: Trimmomatic (v0.36) [33], FastQC (v0.11.9), metaSPAdes (v3.15.3) [34,35], CheckM (v1.0.18) [36], MetaBAT2 Contig Binning (v1.7) [37], CheckM (v1.0.18) [36], extract bins as assemblies from BinnedContigs (v1.0.2) [32], GTDB-Tk (v1.7.0) [38–40], and Kaiju (v1.7.3) [41,42]. GTDB-Tk assigned taxonomies to each MAG by comparing the marker genes of each assembled genome to the Genome Taxonomy Database, which is constructed using RefSeq and Genbank genomes [38]. Kaiju used protein-level classification to assign taxonomies to each sequencing read by comparing read sequences to the NCBI RefSeq database of completely assembled bacterial, archaeal, and viral genomes [41]. Functional gene annotation of MAGs was then performed using FeGenie (v1.2) [43] to identify gene encoding processes involved in Fe metabolism and LithoGenie, an HMM set within MagicLamp (v1.0) [44], to identify other redox genes. Figures were produced in R 4.1.1 [30] using the ggplot2 [28] and cowplot [45] packages.

### 3. Results and Discussion

Batch incubations were prepared using synthetic pore water and pulverized BIF and inoculated with *sub muros* under anaerobic (anoxic) conditions. Two sets of incubations and two sets of uninoculated controls were prepared, and Fe(III) reduction was allowed to proceed. Dissolved and total Fe(II) were measured throughout to quantify Fe(III) reduction. After a period of 91 days, one set of incubations and one set of controls were aerated to simulate the anoxia/oxia cycling that occurs in IFCs (labeled "oxic"). The other incubations and controls remained anoxic for an additional 82 days.

#### 3.1. Fe(III) Reduction under Anoxic Conditions

When BIF was incubated with *sub muros* and remained anoxic, dissolved Fe(II) reached ~2 mM, with a maximum Fe(II) concentration after 37 days (Figure 1A). The variation in both dissolved and total Fe(II) concentrations among these treatments is attributed to the heterogeneity of the *sub muros* and two BIF samples from nearby separate IFCs. Because of the variation and lower values, the dissolved Fe(II) for each replicate was plotted separately, but the total Fe(II) was plotted as an average to represent an average IFC which may contain a variety of BIFs. Dissolved Fe(II) remained at a concentration of 1–2 mM in the anoxic treatment for the remainder of the experiment (Figure 1A). Minimally dissolved Fe(II) accumulated in the uninoculated controls (Figure 1A). Total Fe(II) accumulated to ~8 mmol/L in the anoxic incubations (Figure 1A), with a pH of 6.8 following Fe(III)

reduction, whereas the total Fe(II) in the anoxic controls was 0.5–4.5 mmol/L (Figure 1B) with a pH of 7.3. The pH of the oxic incubations was 7.5 following repeated aeration, suggesting that O<sub>2</sub> exposure slightly increases pH but remains circumneutral. While Fe(III) reduction was halted when O<sub>2</sub> was introduced, the available Fe(II) was not completely oxidized during the 82 days of weekly headspace exchange (Figure 1). The decrease in dissolved Fe(II) indicates that oxidation occurred following aeration, and it is possible that some chemical or microbial interaction, such as Fe(II) sorption/complexation with silica in the BIF, stabilized the solid associated Fe(II) [15,18,19]. The fact that the pH remained circumneutral in both treatments suggests that the amount of Fe(III) reduction in the inoculated samples was not sufficient to affect the pH, as was previously reported [14].

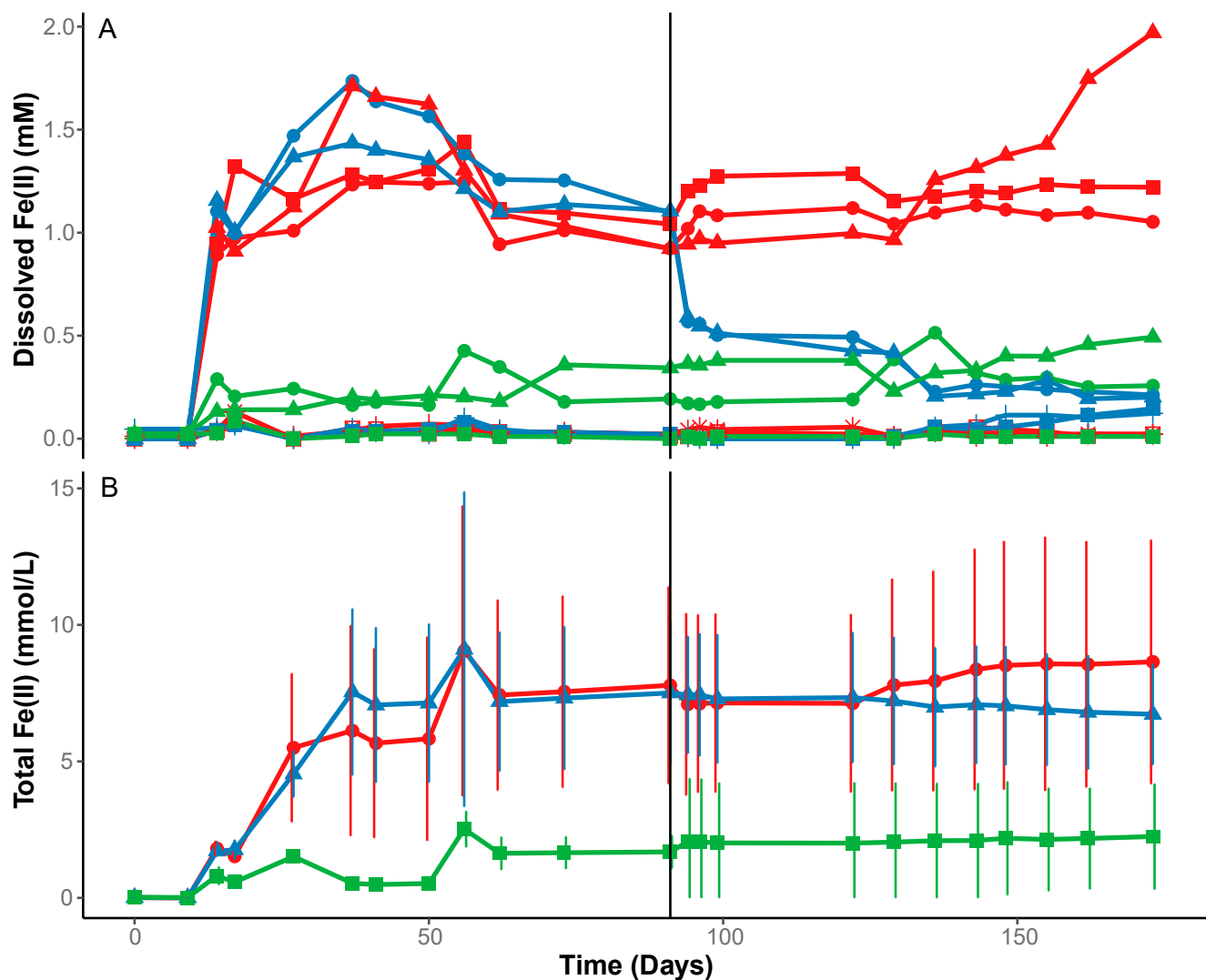


**Figure 1.** Dissolved (A) and total (B) Fe(II) concentrations in uninoculated (green) and *sub micro*-inoculated (red) anoxic incubations. Black vertical line indicates time at 91 days when cultures were aerated (blue). Panel (A) represents dissolved Fe(II) concentrations from replicates of three separate incubations. Panel (B) represents average total Fe(II) concentrations from three separate incubations, with error bars that represent one standard deviation.

In the anoxic treatments, only 1.4% of the total BIF-Fe(III) was reduced, whereas prior experiments using canga as the source of Fe(III) yielded a 3.8% reduction in the total Fe(III) [1,13]. This difference in Fe(III) reduction can be attributed to the differing microbiological reducibility of the Fe(III) phases in BIF versus canga [1]; BIF is primarily composed of hematite, whereas canga is primarily composed of goethite. The reducibility

differences have been attributed to the surface area of crystalline hematite compared to the much higher surface area of poorly crystalline goethite [46]. Because of the variation in O<sub>2</sub> availability that occurs within canga, it is also likely that, at a given time, a significant proportion of reducible Fe(III) may be present as ferrihydrite because of its precipitation from available Fe(II). Ferrihydrite (5 Fe<sub>2</sub>O<sub>3</sub>·9H<sub>2</sub>O) is a poorly ordered Fe(III)-oxide that is likely to be precipitated first and is more reducible than goethite [47,48]. If this was the case, the reducibility of canga would be greater than previous studies have suggested.

Urrutia et al. [19] demonstrated that layered silicates prevented Fe(II) sorption to Fe(III)-oxides and cell surfaces; their results suggest that other Fe(II) ligands, such as humic acids, could have a similar effect. In IFCs, this would mean that the presence of silicates in BIF could prevent Fe(II) sorption to Fe(III)-oxides in BIF, leading to greater extents of Fe(III) reduction. In addition, if Fe(II) is not adsorbed to Fe(III), it can be more easily washed away by groundwater. Wolthoorn et al. [15] found that when anoxic groundwater with a pH > 7 containing PO<sub>4</sub><sup>3-</sup>, Mn, silicate, or fulvic acid was aerated, Fe(II) oxidation was slowed and led to the formation of potentially mobile Fe colloids. In IFCs, because stream waters have circumneutral pH and the host rock is composed of silicate and Fe(III)-oxides, it is likely that Fe(II) traveling in streams or groundwater would oxidize more slowly than if silicate was not present because of the formation of Fe-Si colloids, which are more resistant to Fe(II) oxidation. This may be why there is no significant Fe(II) oxidation occurring in streams, leading to Fe(III)-oxide precipitation and a reduction in stream pH. Similarly, Kinsela et al. [18] found that Fe(II) oxidation was progressively slowed by increasing concentrations of dissolved silicate with a pH range of 6.0–7.0, and the primary Fe(II) oxidation product transitioned from lepidocrocite to a ferrihydrite/silica–ferrihydrite composite. Their results suggest that Fe(II) was sorbed to silica–ferrihydrite solids by weaker, non-specific, outer-sphere sorption complexes compared to lepidocrocite [18]. In IFCs, this could mean that the reason why Fe(II) does not oxidize in streams is because it is weakly sorbed to silica–ferrihydrite solids, making it resistant to oxidation. These studies demonstrate the interactions of Fe(II) and Si, which may lead to slower Fe(II) oxidation rates at a circumneutral pH and may suggest that a similar chemical interaction led to the limited oxidation of solid-associated Fe(II) in this study. These interactions would stabilize Fe(II) in streams/groundwater in IFC environments, allowing Fe(II) mobilization and preventing Fe(II) oxidation in surface streams.

### 3.2. Changes in the Microbial Community Composition

To examine the influence of changing conditions on microbial community profiles, DNA was extracted from *sub muros* and inoculated incubations for 16S rRNA gene sequencing. Illumina iTag sequencing of the *sub muros* inoculum microbial community indicated that it comprised Betaproteobacteria, Gammaproteobacteria, Bacteroidetes, Actinobacteria, and <10% Alphaproteobacteria, Acidobacteria, Chloroflexi, Firmicutes, and Planctomycetes. A past examination of this community revealed an active Fe(III)-reducing community in *sub muros* that appears to be sustained through the oxidation of organic carbon derived from the extensively vegetated soil above [4,13]. After allowing Fe(III) reduction to proceed for several months under anoxic conditions, the microbial community in the *sub muros* appeared to have become dominated by the Firmicutes (97%) (Figure 2), with some Actinobacteria (1.5%) and Proteobacteria (0.3%). The dominant members of the Firmicutes identified were Peptococcaceae, Paenibacillaceae, and Clostridiaceae. However, the dominance of Firmicutes seems to have been overestimated, as can be seen when compared to their abundance of 23% by metagenomic sequencing methods (Figure 3). Previous studies using *sub muros* or other IFC biofilms/sediments have similarly resulted in the enrichment of Firmicutes under Fe(III)-reducing conditions [4,13], although they were not abundant in the initial inoculum. Parker et al. [4] observed a greater extent of Fe(III) reduction when cultures were grown in glucose-containing medium, and Fe(III) reduction was enhanced by the addition of H<sub>2</sub> [4].

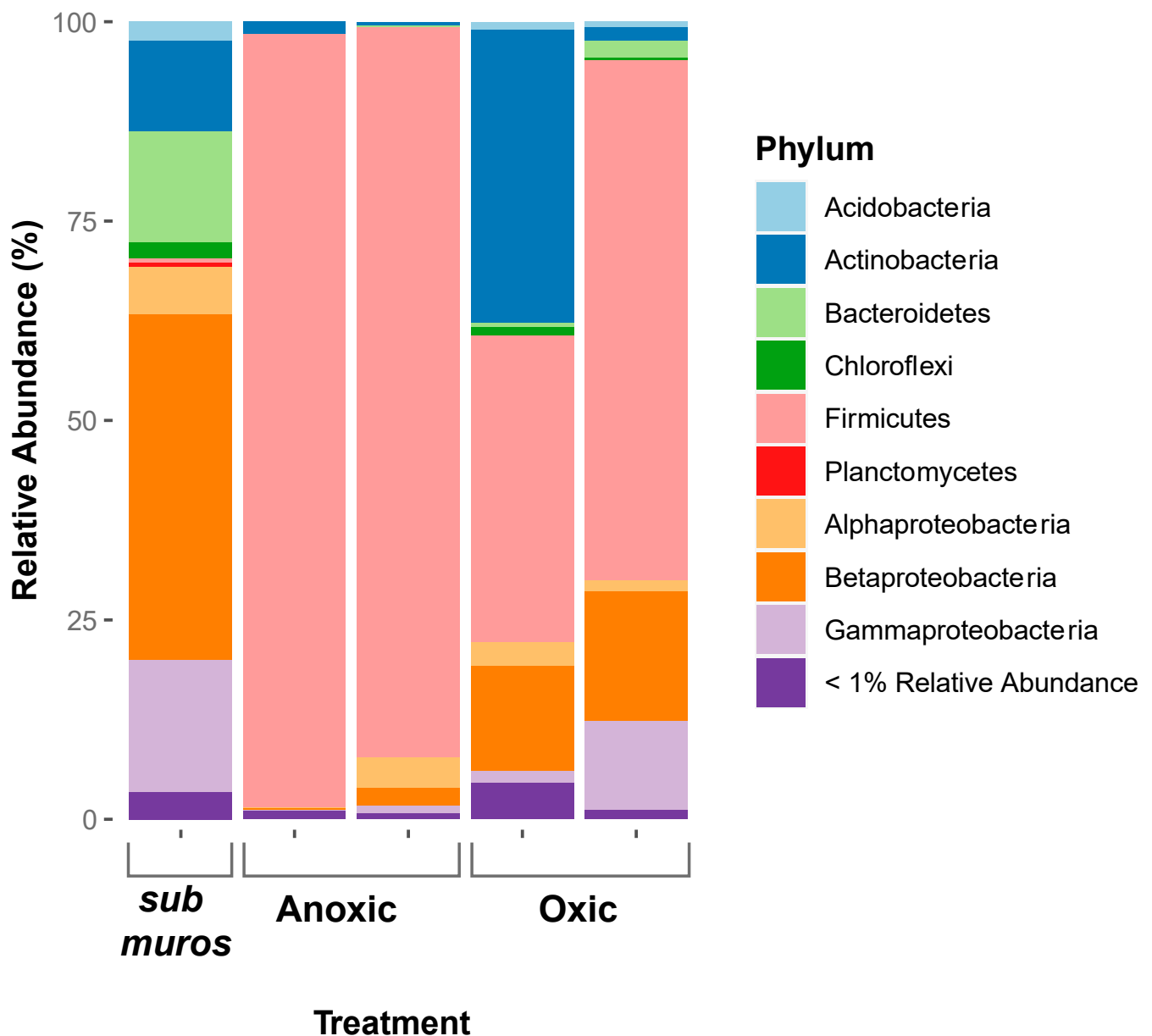


**Figure 2.** Taxonomic distribution of *sub muros* material, anoxic batch incubation, and oxic batch incubation as determined by 16S rRNA iTag sequencing. Shift in microbial diversity represented at phylum level when *sub muros* population was subjected to anoxic, Fe(III)-reducing conditions and when anoxic population was subjected to O<sub>2</sub> exposure. Two replicates from anoxic and oxic batch incubations are included.

When the microbial community was aerated following anoxic incubation for 91 days, the microbial community composition shifted from this Firmicutes-dominated population, showing an increase in members of the Actinobacteria. Oxic cultures showed an increase in Betaproteobacteria (Figure 2). The increase in these phyla along with a reduction in Fe(II) suggests that the community shifted from a fermentative Fe(III)-reducing Firmicutes to a composition more commonly associated with aerobic heterotrophic metabolism.

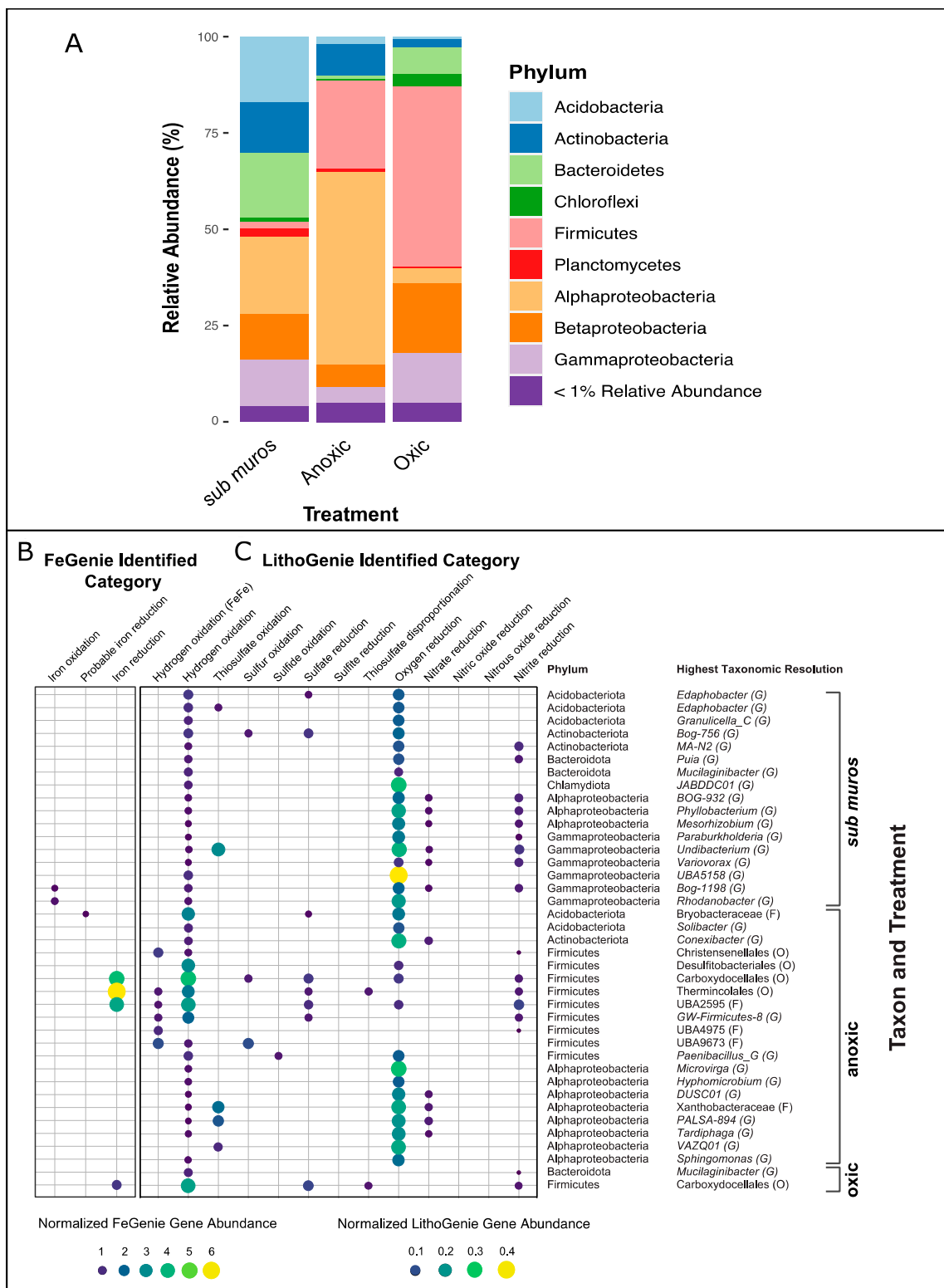


**Figure 3.** Taxonomic distribution from shotgun metagenome read sequences (A) and heatmap of (B) FeGenie-identified Fe reduction/oxidation and (C) LithoGenie-identified reduction/oxidation functional gene summaries identified in *sub muros* material, anoxic batch incubation, and oxic batch incubation MAGs as determined by shotgun metagenome sequencing. Phylum-level taxonomic assignments and highest taxonomic resolution assignments are shown for each MAG. Level of highest taxonomic resolution is represented following assignment where (O) represents order, (F) represents family, and (G) represents genus. Normalized gene abundances are represented by dot size and color.

### 3.3. Metabolic Potential of Anoxic and Oxic Treatments

To understand the metabolic changes that were occurring in the community under the established conditions, we performed metagenomic sequencing. There was an insufficient amount of DNA for metagenomics in the subsamples used for PCR; therefore approximately 6 months after the end of the initial experiment, the entire culture was extracted. Initially, we used metagenomic data to assign taxonomies to the raw sequence reads. Using this approach, the metagenomic sequencing data indicated that the *sub muros* community identified using Kaiju comprised Alphaproteobacteria, Acidobacteria, Bacteroidetes, Actinobacteria, Betaproteobacteria, Gammaproteobacteria, and <5% Firmicutes, Planctomycetes, and Chloroflexi (Figure 3A). Compared to 16S rRNA gene sequencing, taxonomic assignments of our metagenomic reads indicated greater proportions of Alphaproteobacteria and Acidobacteria and a lower proportion of Betaproteobacteria. Other compositional differences between the two sequencing methods were minimal (Figures 2 and 3). These results suggest that some PCR bias occurred when analyzing the *sub muros* or that the community changed slightly during the 6 months between sequencing methods.

There was a lower proportion of Firmicutes, with a community dominated by Alphaproteobacteria (50%), along with Firmicutes (23%), <10% Actinobacteria, Betaproteobacteria, Gammaproteobacteria, and Acidobacteria, when metagenomic read sequencing was used to classify taxonomies in the anoxic community using Kaiju compared to 16S rRNA gene sequencing (Figure 3A). The discrepancy between 16S rRNA gene sequencing and shotgun metagenome sequencing is thought to be due to an overestimation of Clostridia; previous studies have found Clostridia abundances from primer-based sequencing methods to be two to three times that of metagenomic methods [49]. The overestimation of Clostridia by 16S rRNA V4 region amplification may be due to the use of perfectly complementary primers [50]. Nevertheless, Firmicutes make up approximately 23% of the anoxic community based on metagenomic read sequencing, which is higher than that in the *sub muros*, indicating the enrichment of Clostridia regardless of the sequencing method. Bacteroidetes and Planctomycetes were also abundant in the *sub muros* inoculum but were in lower relative abundances upon incubation under anoxic conditions (<1%) (Figures 2 and 3A). In the cultures that were aerated, taxonomic assignments identified using Kaiju based on metagenome sequence reads indicated a similar community structure to that obtained by PCR amplification, with higher relative abundances of the Betaproteobacteria measured by metagenomic sequencing compared to 16S rRNA sequencing. The remainder of the community was composed of <10% Bacteroidetes, Alphaproteobacteria, Chloroflexi, Actinobacteria, Acidobacteria, and Planctomycetes according to metagenomic sequencing using Kaiju (Figure 3A). The differences in relative abundances of Betaproteobacteria and Actinobacteria in oxic incubations between sequencing methods may be due to the community shifting during the months between samplings.

### 3.4. Metagenome Assembled Genome Analyses

We demonstrated the potential for Fe(III) reduction in the *sub muros* community based on metagenomics [14]. To identify which species might be involved in these activities, we analyzed MAGs from the *sub muros* and each treatment. Following quality filtering of metagenomic bins to include only genomes with 80% minimum completeness and 10% maximum contamination, the *sub muros* library included 17 MAGs from the 31 bins, the anoxic library included 20 MAGs from the 41 bins, and the oxic library included 2 MAGs from the 15 bins. Detailed taxonomic classifications of MAGs from GTDB-Tk and quality information from CheckM are shown in Supplementary Table S1. Not all taxonomies identified using read sequences were represented in the MAGs. Some taxa with lower abundances did not result in the development of a MAG, likely due to low sequencing coverage. An analysis of the MAGs from *sub muros* did not reveal any known Fe(III) reduction or probable Fe(III) reduction genes through FeGenie (Figure 3B). Similarly, previous metagenomic analysis of *sub muros* from another IFC did not demonstrate an enrichment in genes associated with iron metabolism, but three MAGs associated with the

Betaproteobacteria, Chloroflexi, and GAL15 were found to encode heme-binding Cys-X-X-Cys-His heme-binding motif-containing proteins [14].

For bacteria to transfer electrons to external compounds, such as Fe(III)-oxides, they must make direct contact with electron acceptors or secrete redox-active mediators [51]. C-type cytochromes are thought to be important mediators in microbial iron reduction by transferring electrons to other multiheme cytochromes and therefore across the periplasm and through the outer membrane [52]. Some bacteria lose their ability to reduce Fe(III)-oxides when certain c-type cytochrome (omcS and omcE) genes are deleted [53]. The importance of c-type cytochromes, such as Cys-X-X-Cys-His, in Fe(III) reduction and the presence of these protein-encoding sequences in past *sub muros* MAGs suggest that extracellular electron transfer and dissimilatory Fe(III) reduction pathways may be present in *sub muros* but involve poorly characterized iron reduction genes.

In this analysis, we also identified the presence of Fe(II) oxidation genes in Alpha- and Gammaproteobacteria MAGs (Figure 3B), and O<sub>2</sub> reduction genes were detected in every MAG (Figure 3C), suggesting the potential for aerobic Fe(II) oxidation, and more broadly, aerobic metabolism in *sub muros*. The lack of genes involved in Fe(III) reduction may be a result of the current limitations of shotgun metagenomic analysis or may indicate that anaerobic metabolisms were not dominant in the *sub muros* at the time of collection, perhaps due to the depletion of Fe(III) in the *sub muros* or the intrusion of O<sub>2</sub> [14]. The latter would suggest that as the reduction in Fe(III) proceeds in *sub muros*, the community shifts in response to Fe(III) availability and may act as an indicator of the maturity of the *sub muros*.

An analysis of the MAGs in the anoxic incubation detected Fe(III)-reducing functional genes in Firmicutes (class Thermicolia, orders Carboxydocellales and Thermicolales) (Figure 3B). Fermentative Firmicutes may use Fe(III)-oxide as an electron sink to maintain redox poise rather than using it as a respiratory substrate [54,55]. They may also form syntrophic relationships with H<sub>2</sub>-consuming, Fe(III)-reducing, or sulfate-reducing organisms, which oxidize H<sub>2</sub> produced by the fermentative organisms to reduce metals [9,54]. The majority of Firmicutes MAGs possess [FeFe] hydrogenases, which catalyze H<sub>2</sub> production [56] from the oxidation of lactate to acetate [57]. The H<sub>2</sub> can then be used as an electron donor for Fe(III) or sulfate reduction [58]. This indicates that fermentative Firmicutes may drive Fe(III) reduction by maintaining redox poise or via interspecies hydrogen transfer to Fe(III) or sulfate reducers. Indeed, previous studies have shown Fe(III) reduction by IFC microbial communities to be enhanced by, rather than limited by, the addition of H<sub>2</sub>, suggesting that hydrogen oxidation has a role in these environments [4]. Lentini et al. [59] proposed fermentative Fe(III) reduction to be more significant than respiratory Fe(III) reduction for the reduction of crystalline Fe(III)-oxides, such as goethite [59]. Fermentative Fe(III) reduction has been implicated in several studies of the iron formation regions of Brazil [4,9,13]. Because the current study and our previous studies have found an abundance of fermentative bacteria and dominance by Firmicutes [4,60], it is likely that fermentative Firmicutes drive Fe(III) reduction in these incubations and possibly in IFCs.

### 3.5. Fe(III)-Reducing Potential of Acidobacteria

Acidobacteria were abundant in the *sub muros* likely due to the acidic conditions there, with a pH of approximately 4.8, which is optimal for the growth of these acidophilic microbes, as indicated by the identities of their MAGs. Interestingly, despite being a relatively small fraction of the anoxic community, we retrieved two MAGs from the Acidobacteria (family *Bryobacteraceae*) from the anoxic incubations (Figure 3). These MAGs contained probable Fe(III) reduction and hydrogenase genes (Figure 3). Given their high abundance in *sub muros* and in IFC biofilm/sediment samples from a previous study [4], Acidobacteria may couple H<sub>2</sub> oxidation with the Fe(III) reduction that occurs in IFCs. Several Acidobacteria can reduce Fe(III), but many of their metabolic processes and ecological functions remain largely unexplored [61,62]. These Fe(III)-reducing Acidobacteria include *Acidobacterium capsulatum* and several other *Acidobacterium*-like isolates [62]. Other

Fe(III)-reducing Acidobacteria include *Geothrix fermentans* [51,63,64]. Some members of *Acidobacteria* also harbor *dsrAB*, which is involved in the reduction of sulfate and other sulfur oxyanions [65–68], which could drive Fe(III) reduction. Indeed, sulfate reduction genes were detected in the Acidobacteria (family *Bryobacteraceae*) MAG (Figure 3C). Given these observations, the abiotic reduction of Fe(III) by biogenic sulfide could be a mechanism of Fe(III) reduction in IFCs, where sulfate and sulfur have been detected [11].

### 3.6. Uncharacterized Fe(III)-Reducing Potential of Alphaproteobacteria

Other components of the microbial community may reduce Fe(III) via uncharacterized metabolic pathways. Several electron transfer strategies involved in Fe(III) reduction remain unclear [69]. For instance, electron transfer via microbial extracellular structures and excreted compounds is not fully understood [69]. Additionally, some operons may contain genes involved in Fe(III) reduction, but due to ambiguities in their function, they are treated with caution as a possible Fe reductase/oxidase by FeGenie [43]. FeGenie can only detect previously documented Fe(III) reduction genes that were used in the development of the FeGenie database hidden Markov models (HMMs). There are no other publicly available HMMs for iron reduction and oxidation genes, with the exception of *mtrB* and *mrtC*, which are in the TIGRFAMS HMM database [43]. As such, there may be other organisms that are capable of Fe(III) reduction but whose genes have not been identified.

Two taxonomic classification tools were used for metagenomic sequence analysis. Kaiju classifies raw sequence reads by assigning each to a taxon in the NCBI taxonomy using protein-level classification, whereas the Genome Taxonomy Database Toolkit (GTDB-Tk) requires binned contigs/assembled genomes and can assign taxonomies to individual MAGs [41]. When metagenomic sequences from the anoxic incubation were taxonomically classified using Kaiju Rhizobiales, Sphingomonadales, Rhodobacterales, and Rhodospirillales were identified as abundant members of the Alphaproteobacteria (Supplementary Figure S1). A relative of the Kaiju-identified Alphaproteobacteria, *Telmatospirillum* (order Rhodospirillales), was recently discovered to possess Fe(III) reduction genes through a metagenome analysis [9]. The MAG of *Telmatospirillum* encodes metal transfer reductases, as well as novel, multi-heme outer membrane cytochromes for extracellular electron transfer, presumably to Fe(III) in canga [9]. Because Fe(III)-reducing members of the Alphaproteobacteria are still being discovered, it is possible that there were Fe(III)-reducing Alphaproteobacteria in our incubations, but Fe(III) reduction genes were not observed because of their novelty. Gagen et al. (2019) used a combination of Prokka, Prodigal, EnrichM, and BLAST to identify Fe(III)-reducing genes in *Telmatospirillum*. The potential Fe(III)-reducing abilities and relatively high abundance in *sub muros* may indicate that members of Alphaproteobacteria contribute to Fe(III) reduction in both IFC environments and our batch incubations.

### 3.7. The Effects of Aeration on the Microbial Community

A goal of this study was to examine the impact of aeration on the community structure and Fe(III)-reducing communities. Metagenomic sequencing of the oxic incubations yielded only two MAGs after quality filtering, likely due to a low DNA yield; however, the species identified were from phyla that were present in both the *sub muros* and anoxic cultures (Figures 2 and 3). Although Fe(II) oxidation genes were detected in two Gammaproteobacteria MAGs within *sub muros*, and following aeration, a similar proportion of Gammaproteobacteria remained (Figure 3A), no Fe(II) oxidation genes were detected in the assembled anoxic MAGs. Nonetheless, the identified Firmicute MAGs retained the genes necessary for Fe(III) reduction (Figure 3B), which may be related to the ability of members of this phylum to sporulate following stressful conditions, meaning the community would maintain the ability to reduce Fe(III) following aeration. MAGs from both anoxic and oxic incubations were identified as Carboxydocellales, and genes necessary for Fe(III) reduction and hydrogen oxidation were identified in these MAGs (Figure 3). The persistence of both genes suggests that Carboxydocellales may couple Fe(III) reduction and hydrogen

oxidation. The identification of hydrogen oxidation genes in nearly every MAG indicates the ability of the community to remove excess  $H_2$  formed during fermentation, avoiding the thermodynamic limitations associated with  $H_2$  accumulation [4,70]. Firmicutes were abundant in anoxic incubations and remained abundant in oxic incubations after several months of  $O_2$  exposure (Figure 3A). These results indicate the rebound potential of the microbial community and their ability to respond to  $O_2$  depletion or availability, allowing them to survive in constantly fluctuating conditions.

### 3.8. Other Metabolic Characteristics of MAGs

There appears to be more to the *sub muros* than just iron metabolism, and the MAG identities of each incubation may provide insights into the other metabolic potentials of the microbial community. MAGs assembled from *sub muros* mostly include members of Acidobacteriaceae (subdivision 1), Actinobacteria, Bacteroidia, Alphaproteobacteria, and Gammaproteobacteria (*Burkholderiaceae* and Xanthomonadales) (Supplementary Table S1). Most of these taxa are widely distributed in soil and are known for their interactions with plant matter.

Acidobacteria are common soil bacteria, and their abundance seems to be correlated with organic carbon availability [71], Subdivision 1 Acidobacteria are abundant in acidic environments, and their abundance is negatively correlated with C, P, and N availability [71,72]. Actinobacteria are widely distributed in soils and are known for their role in plant residue degradation [73]. They have been shown to play key roles in plant residue decomposition despite not dominating the community. MAGs identified as Bacteroidia were classified as either *Sphingobacteriaceae* or *Chitinophagaceae* (Supplementary Table S1); both are diverse families whose members are often found in soil and are associated with plants.

MAGs identified as Alphaproteobacteria included members of *Mesorhizobium*, Azospirillales, *Phyllobacterium*, and others. Members of *Mesorhizobium* and *Azospirillum* are known to form symbiotic relationships with plants and are responsible for nitrogen fixation in root systems [74–76]. *Phyllobacterium* are also associated with plants and are able to reach higher concentrations in warm, moist, and humid tropical environments, like those where IFCs occur [77]. MAGs identified as Gammaproteobacteria included members of *Burkholderiaceae* and Xanthomonadales (Supplementary Table S1). Some members of *Burkholderiaceae* are beneficial to plants, whereas others are pathogenic [78]. Xanthomonadales are diverse, but some are also commonly found in soil and water, and some species are plant pathogens [79,80].

MAGs assembled from anoxic and oxic treatments included many of the same members described above, with the addition of Firmicutes. Firmicutes are associated with the rhizosphere, with some being identified as fermentative organisms, and some found dominating iron-reducing cultures [81–84]. In addition, many Firmicutes can form endospores, allowing them to survive periods of environmental stress and desiccation [85]. This ability would allow Firmicutes to better survive the annual dry season that occurs in Minas Gerais, Brazil and is thought to cause *sub muros* to lose moisture for several months.

The majority of MAGs assembled from *sub muros* belong to taxonomies that are known for their association with plants and soil. This suggests that much of the community enters from the overlying soil or is supported by nutrients from the overlying soil, resulting in the enrichment of these taxa. Because of the heterogeneity and diversity of soil, this results in the complex inoculum (*sub muros*) that we observe in IFCs. This is reflected in the community's ability to shift in response to changes, such as fluctuating  $O_2$  availability, saturation, and carbon availability. The geochemistry of IFCs appears to be profoundly influenced by the soil microbes above, though the details of these interactions and exchanges between the soil microbes and the *sub muros* are currently unclear.

## 4. Conclusions

In this study, we determined the effects of alternating  $O_2$  availability on Fe redox processes and on the *sub muros*-associated microbial community of IFCs to determine whether

the periodic cycling of  $O_2$  into the system is consistent with the proposed mechanism of cave formation, as illustrated in Figure 4. During a period of anoxia, the microbial Fe(III) reduction of BIF-associated Fe(III)-oxides occurred, and members of the Alphaproteobacteria and Firmicutes were enriched; fermentative Firmicutes have been demonstrated to be responsible for Fe(III) reduction observed in previous experiments [4,13]. The detection of sulfate reduction genes in all incubations suggests that sulfate reduction has a significant role, which could occur concurrently with organic carbon fermentation. This process would also drive Fe(III) reduction through an abiotic reaction in which the sulfide produced during sulfate reduction chemically reacts with Fe(III)-oxides, producing Fe(II) and sulfur [86,87] (Figure 4). The enrichment of *Alphaproteobacteria* and the observation of Fe(III) reduction genes in the MAG of *Telmatospirillum* (Rhodospirillales of the Alphaproteobacteria; Gagen, Zaugg et al. (2019)), suggest that Alphaproteobacteria may have reduced Fe(III) in our incubations, but may contain as yet poorly described Fe(III)-reducing genes that were not detected. Although they were not enriched in our anoxic and oxic incubations, Acidobacteria appear to be FeRMs in IFC environments because of their abundance in *sub muros* and other IFC environmental samples, the possession of probable Fe(III) reduction genes in a MAG from anoxic incubation, and because some members are already established as FeRMs [51,62–64].

Following aeration, the partial oxidation of dissolved Fe(II) occurred, but solid-associated Fe(II) oxidation was minimal (Figure 4). It is likely that a chemical sorption/adsorption/complexation interaction stabilized solid-associated Fe(II), preventing complete oxidation. These chemical interactions may stabilize Fe(II), preventing oxidation and allowing mobilization through circumneutral streams (Figure 4). This may be why notable Fe(II) oxidation does not occur in IFC streams and stream water does not become excessively acidic. After the addition of  $O_2$  to anoxic incubations, the community composition shifted from the Firmicutes/Alphaproteobacteria-enriched anoxic community to a community more similar to that found in *sub muros*, which may represent the use of  $O_2$  as the terminal electron acceptor (Figure 4), but maintained the genes necessary for Fe(III) reduction. This suggests that the community, and Firmicutes in particular, can survive  $O_2$  intrusion and return to Fe(III) reduction. Incomplete Fe(II) oxidation combined with the ability of the community to return to reducing Fe(III) after  $O_2$  intrusion suggest a process for enhanced Fe(II) export from IFC systems.

By mimicking the changes in  $O_2$  availability that occur in *sub muros* due to seasonal changes and exogenic biospeleogenetic events, we were able to gain insights into what occurs during these events. We found that anoxia/oxia cycling affected the microbial community, causing it to shift between anaerobic and aerobic processes. Despite this cycling, Fe(III) reduction could proceed during periods of anoxia, and most of the biogenic Fe(II) seemed to be stabilized, likely by interactions with silica, which prevented the oxidation of most of the Fe(II) (Figure 4). Because Fe(II) was not oxidized, it could be mobilized by groundwater, leading to the formation of IFCs in the iron formation regions of Brazil.

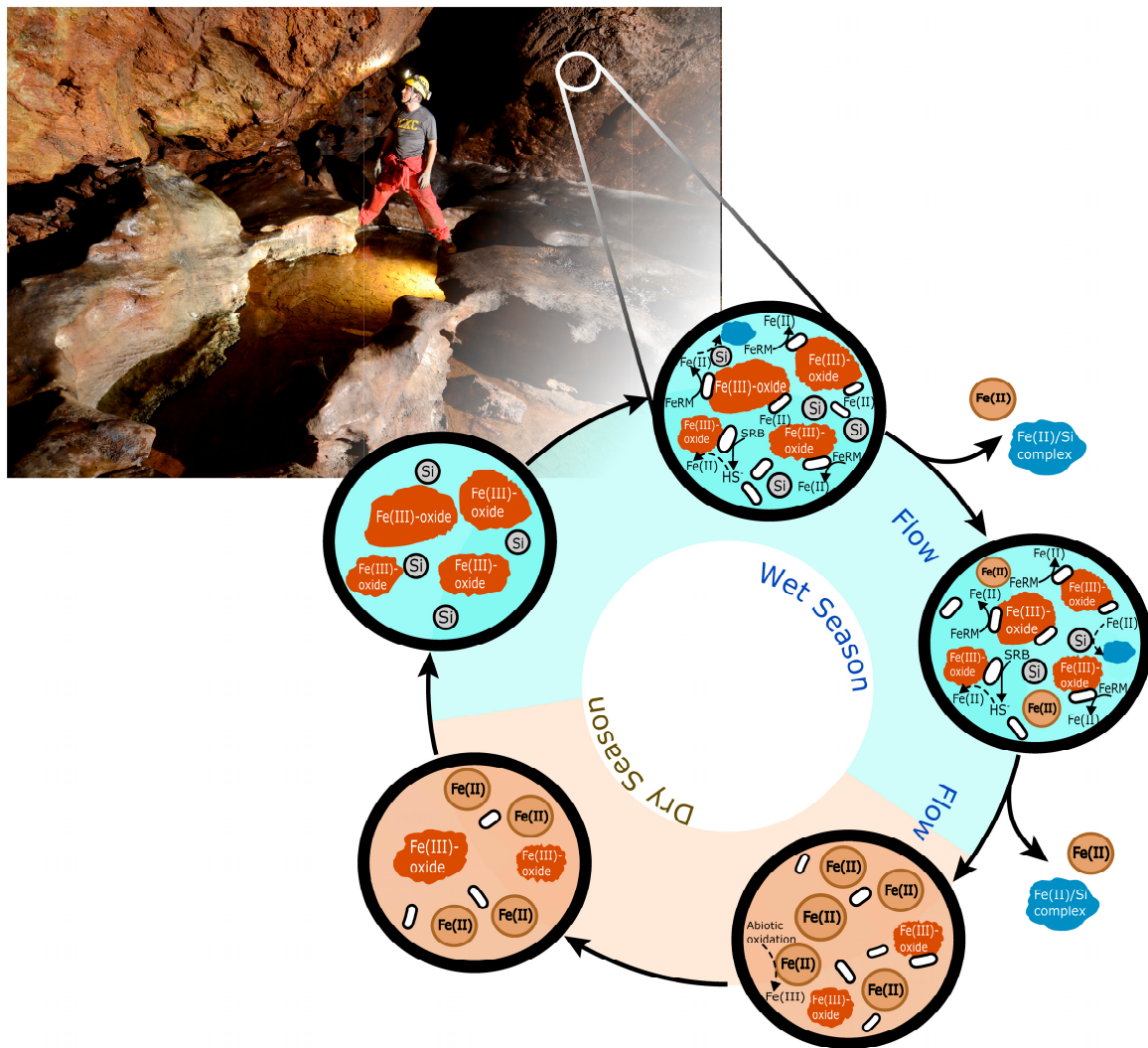


**Figure 4.** Schematic diagram illustrating cyclic geochemical and microbial processes that we propose occur in *sub muros* and which correspond to seasonal changes. Bacterial cells are represented by white ovals. Fe(III)-oxides are illustrated as rust-colored asymmetric shapes, silica/silicates are illustrated as gray circles labeled “Si”, Fe(II)/Si complexes are hypothesized and illustrated as blue asymmetric shapes, and both solid and dissolved Fe(II) are illustrated as tan circles labeled “Fe(II)”. Some microbial reductive processes are shown with solid arrows, while abiotic processes are shown with dashed arrows. Infiltration of organic carbon-rich pore water into *sub muros* during wet season is illustrated as blue “fluid” between minerals and cells. Removal of Fe(II) during rain events is indicated by arrows and “Flow” indicators. Drying of *sub muros* during dry season is illustrated as brown areas around minerals and cells. Photo by Hazel A. Barton.

**Supplementary Materials:** The following supporting information can be downloaded at <https://www.mdpi.com/article/10.3390/min14040425/s1>, Supplementary Figure S1: Taxonomic distribution of *sub muros* material, anoxic batch incubation, and oxic batch incubation as determined by metagenome sequencing. Shift in microbial diversity represented at order-level when *sub muros* population was subjected to anoxic, Fe(III)-reducing conditions and when anoxic population was subjected to O<sub>2</sub> exposure. Supplementary Figure S2: Principal coordinate analysis plot of weighted UniFrac distance of *sub muros* material (green square), anoxic incubation (red circle), and oxic incubation (blue triangle) as determined by QIIME2 analysis of 16S rRNA. Plot shows first two principal coordinates that, when combined, explain 100% of observed genetic variation. Shift in genetic variation represented when *sub muros* population was subjected to anoxic, Fe(III)-reducing conditions and when anoxic population was subjected to O<sub>2</sub> exposure. Supplementary

Data: X-ray diffraction mineral composition results of BIF-containing anoxic, oxic, and uninoculated batch incubations following conclusion of experiment with two replicates of each treatment shown. Results indicate mineral composition of incubations is hematite and quartz, regardless of treatment. Supplementary Data: SEM EDAX csv files showing wt % and atomic % of Si and Fe in BIF samples. Supplementary Table S1: Taxonomic classification and completion/contamination statistics for metagenome-assembled genomes.

**Author Contributions:** Conceptualization, M.K.M., A.S.A., H.A.B. and J.M.S.; methodology, M.K.M., H.A.B. and J.M.S.; formal analysis, M.K.M. and A.M.; investigation, M.K.M. and A.M.; resources, A.S.A., H.A.B. and J.M.S.; data curation, M.K.M.; writing—original draft preparation, M.K.M.; writing—review and editing, A.S.A., H.A.B. and J.M.S.; visualization, M.K.M., A.S.A. and H.A.B.; supervision, H.A.B. and J.M.S.; project administration, H.A.B. and J.M.S.; funding acquisition, H.A.B. and J.M.S. All authors have read and agreed to the published version of the manuscript.

**Funding:** This research was funded by the NSF grant #1645180 from NSF Geobiology and Low-temperature Geochemistry program.

**Data Availability Statement:** The datasets presented in this study can be found in online repositories. Metagenome and 16S rRNA sequence data are available at NCBI under BioProject PRJNA972289.

**Acknowledgments:** We thank Anglo American and the staff of Carste Ciência Ambiental for their support in obtaining cave access and samples. We thank Marina Leão for her assistance in the field and in organizing the sampling efforts. We thank Kayla Calapa, Satoshi Kawaichi, and Ceth Parker for their assistance during sampling. We kindly thank Olivia Hershey for her guidance and support in the genomic analysis.

**Conflicts of Interest:** The authors declare no conflicts of interest.

## References

1. Parker, C.W.; Wolf, J.A.; Auler, A.S.; Barton, H.A.; Senko, J.M. Microbial Reducibility of Fe(III) Phases Associated with the Genesis of Iron Ore Caves in the Iron Quadrangle, Minas Gerais, Brazil. *Minerals* **2013**, *3*, 395–411. [[CrossRef](#)]
2. Shuster, D.L.; Farley, K.A.; Vasconcelos, P.M.; Balco, G.; Monteiro, H.S.; Waltenberg, K.; Stone, J.O. Cosmogenic <sup>3</sup>He in Hematite and Goethite from Brazilian “Canga” Duricrust Demonstrates the Extreme Stability of These Surfaces. *Earth Planet. Sci. Lett.* **2012**, *329–330*, 41–50. [[CrossRef](#)]
3. Dorr, J.V.N. Supergene Iron Ores of Minas Gerais, Brasil. *Econ. Geol.* **1964**, *59*, 1203–1240. [[CrossRef](#)]
4. Parker, C.W.; Auler, A.S.; Barton, M.D.; Sasowsky, I.D.; Senko, J.M.; Barton, H.A. Fe(III) Reducing Microorganisms from Iron Ore Caves Demonstrate Fermentative Fe(III) Reduction and Promote Cave Formation. *Geomicrobiol. J.* **2018**, *35*, 311–322. [[CrossRef](#)]
5. Piló, L.B.; Auler, A. Geoespeleologia das Cavernas em Rochas Ferríferas da Região de Carajas, PA. In Proceedings of the ANAIS do XXX Congresso Brasileiro de Espeleologia, Montes Carlos, Brazil, 9–12 July 2009; pp. 181–186.
6. Auler, A.S.; Parker, C.W.; Barton, H.A.; Soares, G.A. Iron Formation Caves: Genesis and Ecology. In *Encyclopedia of Caves*; Academic Press: Cambridge, MA, USA, 2019; pp. 559–566. [[CrossRef](#)]
7. Auler, A.S.; Piló, L.B.; Parker, C.W.; Senko, J.M.; Sasowsky, I.D.; Barton, H.A. *Hypogene Cave Patterns in Iron Ore Caves: Convergence of Forms or Processes*; Karst Waters Institute Special Publication: Leesburg, VA, USA, 2014; pp. 15–19.
8. Auler, A.S.; Barton, H.A.; Zambelli, B.; Senko, J.; Parker, C.W.; Sasowsky, I.D.; Souza, T.A.R.; Pujoni, D.; Peñaranda, J.; Davis, R. Silica and Iron Mobilization, Cave Development and Landscape Evolution in Iron Formations in Brazil. *Geomorphology* **2022**, *398*, 108068. [[CrossRef](#)]
9. Gagen, E.J.; Zaugg, J.; Tyson, G.W.; Southam, G. Goethite Reduction by a Neutrophilic Member of the Alphaproteobacterial Genus *Telmatospirillum*. *Front. Microbiol.* **2019**, *10*, 02938. [[CrossRef](#)]
10. Levett, A.; Gagen, E.; Shuster, J.; Rintoul, L.; Tobin, M.; Vongsivut, J.; Bamberg, K.; Vasconcelos, P.; Southam, G. Evidence of Biogeochemical Processes in Iron Duricrust Formation. *J. S. Am. Earth Sci.* **2016**, *71*, 131–142. [[CrossRef](#)]
11. Gagen, E.J.; Levett, A.; Paz, A.; Gastauer, M.; Caldeira, C.F.; Valadares, R.B.d.S.; Bitencourt, J.A.P.; Alves, R.; Oliveira, G.; Siqueira, J.O.; et al. Biogeochemical Processes in Canga Ecosystems: Armoring of Iron Ore against Erosion and Importance in Iron Duricrust Restoration in Brazil. *Ore Geol. Rev.* **2019**, *107*, 573–586. [[CrossRef](#)]
12. Levett, A.; Vasconcelos, P.M.; Gagen, E.J.; Rintoul, L.; Spier, C.; Guagliardo, P.; Southam, G. Microbial Weathering Signatures in Lateritic Ferruginous Duricrusts. *Earth Planet. Sci. Lett.* **2020**, *538*, 116209. [[CrossRef](#)]
13. Calapa, K.A.; Mulford, M.K.; Rieman, T.D.; Senko, J.M.; Auler, A.S.; Parker, C.W.; Barton, H.A. Hydrologic Alteration and Enhanced Microbial Reductive Dissolution of Fe(III) (Hydr)Oxides Under Flow Conditions in Fe(III)-Rich Rocks: Contribution to Cave-Forming Processes. *Front. Microbiol.* **2021**, *12*, 696534. [[CrossRef](#)]
14. Parker, C.W.; Senko, J.M.; Auler, A.S.; Sasowsky, I.D.; Schulz, F.; Woyke, T.; Barton, H.A. Enhanced Terrestrial Fe(II) Mobilization Identified through a Novel Mechanism of Microbially Driven Cave Formation in Fe(III)-Rich Rocks. *Sci. Rep.* **2022**, *12*, 17062. [[CrossRef](#)] [[PubMed](#)]

15. Wolthoorn, A.; Temminghoff, E.J.M.; Weng, L.; Van Riemsdijk, W.H. Colloid Formation in Groundwater: Effect of Phosphate, Manganese, Silicate and Dissolved Organic Matter on the Dynamic Heterogeneous Oxidation of Ferrous Iron. *Appl. Geochem.* **2004**, *19*, 611–622. [[CrossRef](#)]
16. Monteiro, H.S.; Vasconcelos, P.M.P.; Farley, K.A. A Combined (U-Th)/He and Cosmogenic <sup>3</sup>He Record of Landscape Armoring by Biogeochemical Iron Cycling. *J. Geophys. Res. Earth Surf.* **2018**, *123*, 298–323. [[CrossRef](#)]
17. Levett, A.; Gagen, E.J.; Vasconcelos, P.M.; Zhao, Y.; Paz, A.; Southam, G. Biogeochemical Cycling of Iron: Implications for Biocementation and Slope Stabilisation. *Sci. Total Environ.* **2020**, *707*, 136128. [[CrossRef](#)] [[PubMed](#)]
18. Kinsela, A.S.; Jones, A.M.; Bligh, M.W.; Pham, A.N.; Collins, R.N.; Harrison, J.J.; Wilsher, K.L.; Payne, T.E.; Waite, T.D. Influence of Dissolved Silicate on Rates of Fe(II) Oxidation. *Environ. Sci. Technol.* **2016**, *50*, 11663–11671. [[CrossRef](#)] [[PubMed](#)]
19. Urrutia, M.M.; Roden, E.E.; Zachara, J.M. Influence of Aqueous and Solid-Phase Fe(II) Complexants on Microbial Reduction of Crystalline Iron(II) Oxides. *Environ. Sci. Technol.* **1999**, *33*, 4022–4028. [[CrossRef](#)]
20. Stookey, L.L. Ferrozine—A New Spectrophotometric Reagent for Iron. *Anal. Chem.* **1970**, *42*, 779–781. [[CrossRef](#)]
21. Caporaso, J.G.; Lauber, C.L.; Walters, W.A.; Berg-Lyons, D.; Lozupone, C.A.; Turnbaugh, P.J.; Fierer, N.; Knight, R. Global Patterns of 16S rRNA Diversity at a Depth of Millions of Sequences per Sample. *Proc. Natl. Acad. Sci. USA* **2011**, *108*, 4516–4522. [[CrossRef](#)] [[PubMed](#)]
22. Bolyen, E.; Rideout, J.R.; Dillon, M.R.; Bokulich, N.A.; Abnet, C.C.; Al-Ghalith, G.A.; Alexander, H.; Alm, E.J.; Arumugam, M.; Asnicar, F.; et al. Reproducible, Interactive, Scalable and Extensible Microbiome Data Science Using QIIME 2. *Nat. Biotechnol.* **2019**, *37*, 852–857. [[CrossRef](#)]
23. Amir, A.; Daniel, M.; Navas-Molina, J.; Kopylova, E.; Morton, J.; Xu, Z.Z.; Eric, K.; Thompson, L.; Hyde, E.; Gonzalez, A.; et al. Deblur Rapidly Resolves Single-Nucleotide Community Sequence Patterns. *Am. Soc. Microbiol.* **2017**, *2*, 10–1128. [[CrossRef](#)]
24. Bokulich, N.A.; Subramanian, S.; Faith, J.J.; Gevers, D.; Gordon, J.I.; Knight, R.; Mills, D.A.; Caporaso, J.G. Quality-Filtering Vastly Improves Diversity Estimates from Illumina Amplicon Sequencing. *Nat. Methods* **2013**, *10*, 57–59. [[CrossRef](#)] [[PubMed](#)]
25. Bokulich, N.A.; Kaehler, B.D.; Rideout, J.R.; Dillon, M.; Bolyen, E.; Knight, R.; Huttley, G.A.; Gregory Caporaso, J. Optimizing Taxonomic Classification of Marker-Gene Amplicon Sequences with QIIME 2's Q2-Feature-Classifer Plugin. *Microbiome* **2018**, *6*, 90. [[CrossRef](#)] [[PubMed](#)]
26. Pedregosa, F.; Varoquaux, G.; Gramfort, A.; Michel, V.; Thirion, B.; Grisel, O.; Blondel, M.; Prettenhofer, P.; Weiss, R.; Dubourg, V.; et al. Scikit-Learn: Machine Learning in Python. *J. Mach. Learn. Res.* **2011**, *12*, 2825–2830.
27. McDonald, D.; Clemente, J.C.; Kuczynski, J.; Rideout, J.R.; Stombaugh, J.; Wendel, D.; Wilke, A.; Huse, S.; Huftnagle, J.; Meyer, F.; et al. The Biological Observation Matrix (BIOM) Format or: How I Learned to Stop Worrying and Love the Ome-Ome. *Gigascience* **2012**, *464*, 2047–217X-1-7. [[CrossRef](#)] [[PubMed](#)]
28. Wickham, H. *Ggplot2: Elegant Graphics for Data Analysis*; Springer: New York, NY, USA, 2016; ISBN 978-3-319-24277-4.
29. Neuwirth, E. *RColorBrewer: ColorBrewer Palettes*; R Foundation for Statistical Computing: Vienna, Austria, 2014.
30. R Core Team. *R: A Language and Environment for Statistical Computing*; R Core Team: Vienna, Austria, 2021.
31. Haendiges, J.; Gonzalez-Escalona, N.; Timme, R.; Balkey, M. Illumina DNA Prep (M) Tagmentation Library Preparation for Use on an Illumina MiSeq Sequencer. 2020. Available online: [https://www.researchgate.net/publication/354560175\\_Illumina\\_DNA\\_Prepare\\_M\\_Tagmentation\\_Library\\_Preparation\\_for\\_use\\_on\\_an\\_Illumina\\_MiSeq\\_Sequencer\\_v2](https://www.researchgate.net/publication/354560175_Illumina_DNA_Prepare_M_Tagmentation_Library_Preparation_for_use_on_an_Illumina_MiSeq_Sequencer_v2) (accessed on 14 April 2022).
32. Arkin, A.P.; Cottingham, R.W.; Henry, C.S.; Harris, N.L.; Stevens, R.L.; Maslov, S.; Dehal, P.; Ware, D.; Perez, F.; Canon, S.; et al. KBase: The United States Department of Energy Systems Biology Knowledgebase. *Nat. Biotechnol.* **2018**, *36*, 566–569. [[CrossRef](#)] [[PubMed](#)]
33. Bolger, A.M.; Lohse, M.; Usadel, B. Trimmomatic: A Flexible Trimmer for Illumina Sequence Data. *Bioinformatics* **2014**, *30*, 2114–2120. [[CrossRef](#)]
34. Pribelski, A.; Antipov, D.; Meleshko, D.; Lapidus, A.; Korobeynikov, A. Using SPAdes De Novo Assembler. *Curr. Protoc. Bioinform.* **2020**, *70*, e102. [[CrossRef](#)]
35. Nurk, S.; Meleshko, D.; Korobeynikov, A.; Pevzner, P.A. MetaSPAdes: A New Versatile Metagenomic Assembler. *Genome Res.* **2017**, *27*, 824–834. [[CrossRef](#)]
36. Parks, D.H.; Imelfort, M.; Skennerton, C.T.; Hugenholtz, P.; Tyson, G.W. CheckM: Assessing the Quality of Microbial Genomes Recovered from Isolates, Single Cells, and Metagenomes. *Genome Res.* **2015**, *25*, 1043–1055. [[CrossRef](#)]
37. Kang, D.D.; Froula, J.; Egan, R.; Wang, Z. MetaBAT, an Efficient Tool for Accurately Reconstructing Single Genomes from Complex Microbial Communities. *PeerJ* **2015**, *3*, e1165. [[CrossRef](#)]
38. Chaumeil, P.; Mussing, A.; Hugenholtz, P.; Parks, D. GTDB-Tk: A Toolkit to Classify Genomes with the Genome Taxonomy Database. *Bioinformatics* **2019**, *36*, 1925–1927. [[CrossRef](#)]
39. Parks, D.H.; Chuvochina, M.; Chaumeil, P.-A.; Rinke, C.; Mussig, A.J.; Hugenholtz, P. A Complete Domain-to-Species Taxonomy for Bacteria and Archaea. *Nat. Biotechnol.* **2020**, *38*, 1079–1086. [[CrossRef](#)] [[PubMed](#)]
40. Parks, D.H.; Chuvochina, M.; Waite, D.W.; Rinke, C.; Skarshewski, A.; Chaumeil, P.-A.; Hugenholtz, P. A Standardized Bacterial Taxonomy Based on Genome Phylogeny Substantially Revises the Tree of Life. *Nat. Biotechnol.* **2018**, *36*, 996–1004. [[CrossRef](#)] [[PubMed](#)]
41. Menzel, P.; Ng, K.L.; Krogh, A. Fast and Sensitive Taxonomic Classification for Metagenomics with Kaiju. *Nat. Commun.* **2016**, *7*, 11257. [[CrossRef](#)] [[PubMed](#)]

42. Ondov, B.D.; Bergman, N.H.; Phillippy, A.M. Interactive Metagenomic Visualization in a Web Browser. *BMC Bioinform.* **2011**, *12*, 385. [CrossRef] [PubMed]
43. Garber, A.I.; Nealson, K.H.; Okamoto, A.; McAllister, S.M.; Chan, C.S.; Barco, R.A.; Merino, N. FeGenie: A Comprehensive Tool for the Identification of Iron Genes and Iron Gene Neighborhoods in Genome and Metagenome Assemblies. *Front. Microbiol.* **2020**, *11*, 37. [CrossRef] [PubMed]
44. Garber, A.I.; Ramirez, G.; Merino, N.; Pavia, M.; McAllister, S. MagicLamp: Toolkit for Annotation of 'omics Datasets Using Curated HMM Sets. 2020. Available online: <https://github.com/Arkadiy-Garber/MagicLamp> (accessed on 14 April 2022).
45. Wilke, C.O. *Cowplot: Streamlined Plot Theme and Plot Annotations for "Ggplot2"*; R Core Team: Vienna, Austria, 2020.
46. Roden, E.E.; Zachara, J.M. Microbial Reduction of Crystalline Iron(III) Oxides: Influence of Oxide Surface Area and Potential for Cell Growth. *Environ. Sci. Technol.* **1996**, *30*, 1618–1628. [CrossRef]
47. Roden, E.E.; Urrutia, M.M. Ferrous Iron Removal Promotes Microbial Reduction of Crystalline Iron(III) Oxides. *Environ. Sci. Technol.* **1999**, *33*, 1847–1853. [CrossRef]
48. Vu, H.P.; Shaw, S.; Brinza, L.; Benning, L.G. Crystallization of Hematite ( $\alpha$ -Fe<sub>2</sub>O<sub>3</sub>) under Alkaline Condition: The Effects of Pb. *Cryst. Growth Des.* **2010**, *10*, 1544–1551. [CrossRef]
49. Fischer, M.A.; Güllert, S.; Neulinger, S.C.; Streit, W.R.; Schmitz, R.A. Evaluation of 16S rRNA Gene Primer Pairs for Monitoring Microbial Community Structures Showed High Reproducibility within and Low Comparability between Datasets Generated with Multiple Archaeal and Bacterial Primer Pairs. *Front. Microbiol.* **2016**, *7*, 211583. [CrossRef]
50. Jovel, J.; Patterson, J.; Wang, W.; Hotte, N.; O'Keefe, S.; Mitchel, T.; Perry, T.; Kao, D.; Mason, A.L.; Madsen, K.L.; et al. Characterization of the Gut Microbiome Using 16S or Shotgun Metagenomics. *Front. Microbiol.* **2016**, *7*, 459. [CrossRef] [PubMed]
51. Mehta-Kolte, M.G.; Bond, D.R. *Geothrix Fermentans* Secretes Two Different Redox-Active Compounds to Utilize Electron Acceptors across a Wide Range of Redox Potentials. *Appl. Environ. Microbiol.* **2012**, *78*, 6987–6995. [CrossRef] [PubMed]
52. Fuller, S.J.; McMillan, D.G.G.; Renz, M.B.; Schmidt, M.; Burke, I.T.; Stewart, D.I. Extracellular Electron Transport-Mediated Fe(III) Reduction by a Community of Alkaliphilic Bacteria That Use Flavins as Electron Shuttles. *Appl. Environ. Microbiol.* **2014**, *80*, 128–137. [CrossRef] [PubMed]
53. Mehta, T.; Coppi, M.V.; Childers, S.E.; Lovley, D.R. Outer Membrane C-Type Cytochromes Required for Fe(III) and Mn(IV) Oxide Reduction in *Geobacter Sulfurreducens*. *Appl. Environ. Microbiol.* **2005**, *71*, 8634–8641. [CrossRef] [PubMed]
54. Shah, M.; Lin, C.C.; Kukkadapu, R.; Engelhard, M.H.; Zhao, X.; Wang, Y.; Barkay, T.; Yee, N. Syntrophic Effects in a Subsurface Clostridial Consortium on Fe(III)-(Oxyhydr)Oxide Reduction and Secondary Mineralization. *Geomicrobiol. J.* **2014**, *31*, 101–115. [CrossRef]
55. List, C.; Hosseini, Z.; Lederballe Meibom, K.; Hatzimanikatis, V.; Bernier-Latmani, R. Impact of Iron Reduction on the Metabolism of *Clostridium acetobutylicum*. *Environ. Microbiol.* **2019**, *21*, 3548–3563. [CrossRef] [PubMed]
56. Morra, S. Fantastic [FeFe]-Hydrogenases and Where to Find Them. *Front. Microbiol.* **2022**, *13*, 853626. [CrossRef] [PubMed]
57. Van den Berg, W.A.M.; Van Dongen, W.M.A.M.; Veeger, C. Reduction of the Amount of Periplasmic Hydrogenase in *Desulfovibrio vulgaris* (Hildenborough) with Antisense RNA: Direct Evidence for an Important Role of This Hydrogenase in Lactate Metabolism. *J. Bacteriol.* **1991**, *173*, 3688–3694. [CrossRef] [PubMed]
58. Zhou, C.; Zhou, Y.; Rittmann, B.E. Reductive Precipitation of Sulfate and Soluble Fe(III) by *Desulfovibrio vulgaris*: Electron Donor Regulates Intracellular Electron Flow and Nano-FeS Crystallization. *Water Res.* **2017**, *119*, 91–101. [CrossRef]
59. Lentini, C.J.; Wankel, S.D.; Hansel, C.M. Enriched Iron(III)-Reducing Bacterial Communities Are Shaped by Carbon Substrate and Iron Oxide Mineralogy. *Front. Microbiol.* **2012**, *3*, 36789. [CrossRef]
60. Parker, C.W.; Senko, J.; Sasowsky, I.D.; Auler, A.; Barton, H.A. Can Fermenting Bacteria Drive Speleogenesis in Fe(III)-Rich Rocks? In Proceedings of the Union Internationale de Speleologie 17th Annuyal International Congress of Speleology, Sydney, Australia, 23–29 July 2017; pp. 399–400.
61. Kalam, S.; Basu, A.; Ahmad, I.; Sayyed, R.Z.; El-Enshasy, H.A.; Dailin, D.J.; Suriani, N.L. Recent Understanding of Soil Acidobacteria and Their Ecological Significance: A Critical Review. *Front. Microbiol.* **2020**, *11*, 580024. [CrossRef]
62. Coupland, K.; Johnson, D.B. Evidence That the Potential for Dissimilatory Ferric Iron Reduction Is Widespread among Acidophilic Heterotrophic Bacteria. *FEMS Microbiol. Lett.* **2008**, *279*, 30–35. [CrossRef] [PubMed]
63. Nevin, K.P.; Lovley, D.R. Mechanisms for Accessing Insoluble Fe(III) Oxide during Dissimilatory Fe(III) Reduction by *Geothrix fermentans*. *Appl. Environ. Microbiol.* **2002**, *68*, 2294–2299. [CrossRef] [PubMed]
64. Coates, J.D.; Ellis, D.J.; Gaw, C.V.; Lovley, D.R. *Geothrix fermentans* gen. nov., sp. nov., a Novel Fe(III)-Reducing Bacterium from a Hydrocarbon-Contaminated Aquifer. *Int. J. Syst. Bacteriol.* **1999**, *49*, 1615–1622. [CrossRef] [PubMed]
65. Huang, S.; Vieira, S.; Bunk, B.; Riedel, T.; Spröer, C.; Overmann, J. First Complete Genome Sequence of a Subdivision 6 *Acidobacterium* Strain. *Genome Announc.* **2016**, *4*, 10-1128. [CrossRef]
66. Wasmund, K.; Mußmann, M.; Loy, A. The Life Sulfuric: Microbial Ecology of Sulfur Cycling in Marine Sediments. *Environ. Microbiol. Rep.* **2017**, *9*, 323–344. [CrossRef]
67. Anantharaman, K.; Hausmann, B.; Jungbluth, S.P.; Kantor, R.S.; Lavy, A.; Warren, L.A.; Rappé, M.S.; Pester, M.; Loy, A.; Thomas, B.C.; et al. Expanded Diversity of Microbial Groups That Shape the Dissimilatory Sulfur Cycle. *ISME J.* **2018**, *12*, 1715–1728. [CrossRef]
68. Hausmann, B.; Pelikan, C.; Herbold, C.W.; Köstlbacher, S.; Albertsen, M.; Eichorst, S.A.; Glavina Del Rio, T.; Huemer, M.; Nielsen, P.H.; Rattei, T.; et al. Peatland *Acidobacteria* with a Dissimilatory Sulfur Metabolism. *ISME J.* **2018**, *12*, 1729–1742. [CrossRef]

69. Kappler, A.; Bryce, C.; Mansor, M.; Lueder, U.; Byrne, J.M.; Swanner, E.D. An Evolving View on Biogeochemical Cycling of Iron. *Nat. Rev. Microbiol.* **2021**, *19*, 360–374. [[CrossRef](#)]
70. Jackson, B.E.; McInerney, M.J. Anaerobic Microbial Metabolism Can Proceed Close to Thermodynamic Limits. *Nature* **2002**, *415*, 454–456. [[CrossRef](#)]
71. Kielak, A.M.; Barreto, C.C.; Kowalchuk, G.A.; van Veen, J.A.; Kuramae, E.E. The Ecology of *Acidobacteria*: Moving beyond Genes and Genomes. *Front. Microbiol.* **2016**, *7*, 171794. [[CrossRef](#)] [[PubMed](#)]
72. Sait, M.; Davis, K.E.R.; Janssen, P.H. Effect of PH on Isolation and Distribution of Members of Subdivision 1 of the Phylum *Acidobacteria* Occurring in Soil. *Appl. Environ. Microbiol.* **2006**, *72*, 1852–1857. [[CrossRef](#)] [[PubMed](#)]
73. Bao, Y.; Dolfig, J.; Guo, Z.; Chen, R.; Wu, M.; Li, Z.; Lin, X.; Feng, Y. Important Ecophysiological Roles of Non-Dominant *Actinobacteria* in Plant Residue Decomposition, Especially in Less Fertile Soils. *Microbiome* **2021**, *9*, 84. [[CrossRef](#)] [[PubMed](#)]
74. Maheshwari, P.; Sankar, P.M. Culture-Independent and Culture-Dependent Approaches in Symbiont Analysis. In *Microbial Symbionts*; Elsevier: Amsterdam, The Netherlands, 2023; pp. 743–763.
75. Pallardy, S.G. Nitrogen Metabolism. In *Physiology of Woody Plants*; Elsevier: Amsterdam, The Netherlands, 2008; pp. 233–254.
76. Steenhoudt, O.; Vanderleyden, J. Azospirillum, a Free-Living Nitrogen-Fixing Bacterium Closely Associated with Grasses: Genetic, Biochemical and Ecological Aspects. *FEMS Microbiol. Rev.* **2000**, *24*, 487–506. [[CrossRef](#)] [[PubMed](#)]
77. Coutinho, T.A.; Bophela, K.N. Tree Leaves as a Habitat for phyllobacteria. In *Forest Microbiology*; Elsevier: Amsterdam, The Netherlands, 2021; pp. 133–144.
78. Compant, S.; Nowak, J.; Coenye, T.; Clément, C.; Ait Barka, E. Diversity and Occurrence of *Burkholderia* spp. in the Natural Environment. *FEMS Microbiol. Rev.* **2008**, *32*, 607–626. [[CrossRef](#)]
79. Pidot, S.J.; Coyne, S.; Kloss, F.; Hertweck, C. Antibiotics from Neglected Bacterial Sources. *Int. J. Med. Microbiol.* **2014**, *304*, 14–22. [[CrossRef](#)] [[PubMed](#)]
80. Bayer-Santos, E.; DeMoraes Ceseti, L.; Farah, C.S.; Alvarez-Martinez, C.E. Distribution, Function and Regulation of Type 6 Secretion Systems of Xanthomonadales. *Front. Microbiol.* **2019**, *10*, 458221. [[CrossRef](#)]
81. Borriss, R. Bacillus. In *Beneficial Microbes in Agro-Ecology*; Elsevier: Amsterdam, The Netherlands, 2020; pp. 107–132.
82. Pan, Y.; Yang, X.; Xu, M.; Sun, G. The Role of Enriched Microbial Consortium on Iron-Reducing Bioaugmentation in Sediments. *Front. Microbiol.* **2017**, *8*, 462. [[CrossRef](#)] [[PubMed](#)]
83. Lovley, D.R.; Holmes, D.E.; Nevin, K.P. Dissimilatory Fe(III) and Mn(IV) Reduction. *Adv. Microb. Physiol.* **1991**, *49*, 219–286. [[CrossRef](#)]
84. Gapes, J.R. Economics of AB Fermentation 27 The Economics of Acetone-Butanol Fermentation: Theoretical and Market Considerations Fermentation Symposium JMMB Minireview. *J. Mol. Microbiol. Biotechnol.* **2000**, *2*, 27–32.
85. Parkes, R.J.; Sass, H. Deep Sub-Surface. In *Encyclopedia of Microbiology*; Elsevier: Amsterdam, The Netherlands, 2009; pp. 64–79.
86. Adriaens, P.; Gruden, C.; McCormick, M.L. Biogeochemistry of Halogenated Hydrocarbons. *Treatise Geochem.* **2003**, *9*, 612. [[CrossRef](#)]
87. Hansel, C.M.; Lentini, C.J.; Tang, Y.; Johnston, D.T.; Wankel, S.D.; Jardine, P.M. Dominance of Sulfur-Fueled Iron Oxide Reduction in Low-Sulfate Freshwater Sediments. *ISME J.* **2015**, *9*, 2400–2412. [[CrossRef](#)] [[PubMed](#)]

**Disclaimer/Publisher’s Note:** The statements, opinions and data contained in all publications are solely those of the individual author(s) and contributor(s) and not of MDPI and/or the editor(s). MDPI and/or the editor(s) disclaim responsibility for any injury to people or property resulting from any ideas, methods, instructions or products referred to in the content.